Variable-Temperature, Variable-Field Magnetic Circular Dichroism Spectroscopic Study of the Metal Clusters in the Δ*nifB* and Δ*nifH* MoFe Proteins of Nitrogenase from *Azotobacter vinelandii*†

Robyn B. Broach,‡ Kresimir Rupnik,‡ Yilin Hu,§ Aaron W. Fay,§ Marcia Cotton,‡ Markus W. Ribbe,*,§ and Brian J. Hales*,‡

Department of Molecular Biology and Biochemistry, University of California, Irvine, California 92697-3900, and Department of Chemistry, Louisiana State University, Baton Rouge, Louisiana 70803-1804

Received August 19, 2006; Revised Manuscript Received October 3, 2006

ABSTRACT: Deletion of *nifB* results in the formation of a variant nitrogenase MoFe protein (Δ*nifB* MoFe protein) that appears to contain two normal [8Fe-7S] P clusters. This protein can be reactivated to form the holo MoFe protein upon addition of isolated FeMo cofactor. In contrast, deletion of *nifH* results in a variant protein (Δ*nifH* MoFe protein) that appears to contain FeS clusters different from the normal P cluster, presumably representing precursors of the normal P cluster. The Δ*nifH* MoFe protein is not reconstituted to the holo MoFe protein with isolated FeMo cofactor. The EPR and EXAFS spectroscopic properties of FeS clusters in the Δ*nifH* MoFe protein clearly differ from those of the normal P cluster found in the Δ*nifB* MoFe protein and suggest the presence of [4Fe-4S]-like clusters. To further characterize the metal cluster structures in the Δ*nifH* MoFe protein, a variable-temperature, variable-field magnetic circular dichroism (VTVH-MCD) spectroscopic study has been undertaken on both the Δ*nifB* MoFe protein and the Δ*nifH* MoFe protein in both the dithionite-reduced and oxidized states. This study clearly shows that each half of the dithionite-reduced Δ*nifH* MoFe protein contains a $[4Fe\text{-}4S]^{+}$ cluster paired with a diamagnetic [4Fe-4S]-like cluster. Upon oxidation, the VTVH-MCD spectrum of the Δ*nifH* MoFe protein reveals a paramagnetic, albeit EPR-silent system, suggesting an integer spin state. These results suggest that the Δ*nifH* MoFe protein contains a pair of neighboring, unusual [4Fe-4S]-like clusters, which are paramagnetic in their oxidized state.

Nitrogenase is a metalloenzyme that catalyzes the reduction of dinitrogen to ammonia (for recent reviews see refs *1*−*7*).[1] This enzyme is composed of two separately purifiable proteins, the iron (Fe) and the molybdenum−iron (MoFe) protein. The homodimeric Fe protein couples ATP hydrolysis to interprotein electron transfer during substrate reduction, serving as an obligate electron donor to the catalytically active component, the MoFe protein. The $\alpha_2\beta_2$ tetrameric MoFe protein contains two copies of unique metal clusters, designated the P cluster[2] and the iron−molybdenum cofactor, respectively. The [8Fe-7S] P cluster (*8*) likely participates in interprotein electron transfer, whereas the FeMo cofactor (*9*) serves as the active site of substrate binding and reduction.

For decades, the biosynthetic mechanism of the two metal clusters of the MoFe protein has attracted considerable interest, not only because these clusters are important for N_2 fixation but also because successful chemical synthesis of these clusters has remained elusive so far. The FeMo cofactor is a heterometallic double cubane comprising one [4Fe-3S] and one [Mo-3Fe-3S] partial cubane, bridged by three sulfides that share a common μ_6 central atom whose identity is unknown but is considered to be C, O, or N (*9*). Located entirely in the α subunit, the FeMo cofactor is bridged to the protein by only two ligands, a cysteine that is bound to the iron at one end of the cluster and a histidine that is bound to the molybdenum at the opposite end of the

† This work was supported by National Institutes of Health Grant GM-67626 (M.W.R.) and the USDA, 2003-02105 NRI, CSREES (B.J.H.).

* Corresponding authors. M.W.R.: e-mail, mribbe@uci.edu; tel, 949-824-9509; fax, 949-824-8551. B.J.H.: e-mail, bhales@lsu.edu; tel, 225-578-4694; fax, 225-578-3458.

‡ Louisiana State University.

§ University of California.

[1] Four classes of nitrogenases have been described. They are the molybdenum nitrogenase, the vanadium nitrogenase, the iron-only nitrogenase, and the nitrogenase of *Streptomyces thermoautotrophicus*. The major distinctive feature of the first three classes of nitrogenases, which are otherwise very similar, is the heterometal atom in the active site of the metal cluster (molybdenum, vanadium, and iron, respectively). The fourth nitrogenase is superoxide-dependent and is apparently different from the other nitrogenase classes (*35*). The molybdenum nitrogenase discussed herein is considered to be the "conventional" nitrogenase. The biosynthesis of the component proteins of the molybdenum nitrogenase and their containing metalloclusters are controlled by the nitrogen fixation (*nif*) genes (for recent reviews see refs *11* and *36*).

[2] Abbreviations: Av1, MoFe protein from *Azotobacter vinelandii*; Kp1, MoFe Protein from *Klebsiella pneumoniae*; P cluster, Fe_8S_7 cluster located in the MoFe protein; *nifB*, gene used to encode a protein needed in the initial steps in FeMo cofactor synthesis; *nifH*, gene used to encode for the polypeptide of the Fe protein (the gene product is also involved in FeMo cofactor maturation and insertion into the apo MoFe protein); VTVH-MCD, variable-temperature, variable-field magnetic circular dichroism; IDS, indigodisulfonic acid; NifEN, protein encoded by the *nifE* and *nifN* genes and proposed to function as a scaffold for the formation of the FeMo cofactor; EXAFS, extended X-ray absorption fine structure.

10.1021/bi061697p CCC: $33.50
Published on Web 11/18/2006

cluster. The molybdenum is also coordinated by homocitrate. The P cluster, with a topology similar to that of the FeMo cofactor, consists of a symmetric double cubane in which two [4Fe-3S] partial cubanes share a central μ_6 sulfur atom (*8*). It is located between the $\alpha\beta$ dimeric interface and is connected to the protein through six cysteine ligands, two terminal and one bridging cysteine from each subunit. The P cluster can be reversibly oxidized from this native, all ferrous state, designated P^N, with indigodisulfonate (IDS), to yield a two-electron oxidized state, designated P^{OX} or P^{2+}. Following a redox-dependent conformational change, the [4Fe-4S] cube associated with the α subunit is largely unchanged, whereas the [4Fe-4S] cube associated with the β subunit is opened concomitant with a decrease in the coordination of the central sulfur atom from six to four (*8*, *10*). The two iron atoms that are no longer coordinated by the central sulfur in the P^{OX} state remain four-coordinate by forming new bonds, one with the alkoxy group of a neighboring serine and the other with a backbone amide group of a bridging cysteine (*8*, *10*).

Despite the progress in elucidating the biosynthesis and insertion mechanism of the FeMo cofactor (*11*), the assembly of the P cluster remains largely unknown. Two types of FeMo cofactor-deficient MoFe protein variants, obtained through either *nifB* or *nifH* deletion, have allowed studies of P cluster species without the interference of the FeMo cofactor (*12*−*15*). Deletion of *nifB* gene, the product of which is the starting point of FeMo cofactor biosynthesis (*11*), does not affect P cluster formation, and the resulting MoFe protein variant contains intact P clusters (*12*, *13*). Interestingly, deletion of the *nifH* gene, the product of which has been established to be involved in FeMo cofactor biosynthesis (*11*), also has an effect on the formation of the P cluster (*14*, *15*). A recent study based on Fe K-edge X-ray absorption (XAS) edge and extended fine structure (EXAFS) showed that a MoFe protein variant isolated from a *nifH* deletion strain of *Azotobacter vinelandii* (designated Δ*nifH* MoFe protein) does not contain a fully assembled P cluster; rather, it has a P cluster precursor that is composed of two [4Fe-4S]-like clusters (*14*). Three different types of structural models were proposed as the most plausible structure of the P cluster precursor, all of which were consistent with biochemical (*15*) and electronic evidence (*14*): (i) two completely separated [4Fe-4S] centers, (ii) two [4Fe-4S] center fragments which are bridged by one cysteine, and (iii) an edge-bridged [8Fe-8S] double cubane (*14*). These results provide the first insights into the process of P cluster formation, which occurs likely by the condensation or rearrangement of two [4Fe-4S]-like fragments, possibly concomitant with Fe protein (*nifH* gene product) induced conformational change (*14*).

Due to the absence of crystal structures, it is impossible to exclude any of the three structural models of the P cluster precursor in the Δ*nifH* MoFe protein and further establish the exact function of the Fe protein in the P cluster assembly. Here we report a comparative variable-temperature, variable-field magnetic circular dichroism (VTVH-MCD) spectroscopic study comparing the metal clusters of Δ*nifH* and Δ*nifB* MoFe proteins in both as-isolated and oxidized states. These spectra clearly show electronic differences between the two protein forms. The as-isolated Δ*nifB* MoFe protein possesses a featureless MCD spectrum dominated by **B**-term contributions associated with a diamagnetic ground state. The MCD spectrum of the as-isolated Δ*nifH* MoFe protein arises from **C**-term contribution clearly associated with a paramagnetic $[4Fe\text{-}4S]^+$ cluster. Following oxidation, the clusters in both proteins are paramagnetic. In the Δ*nifB* MoFe protein, the paramagnetism arises from the P^{OX} integer spin state. The paramagnetism in the oxidized Δ*nifH* MoFe protein presumably also arises from an integer state most likely associated with neighboring, spin-coupled [4Fe-4S]-like clusters. This structural characterization of the Δ*nifH* MoFe protein means that the clusters of this protein do not behave like typical ferredoxin clusters and gives further insight into the chemical synthesis and processing of the MoFe protein P clusters.

MATERIALS AND METHODS

Unless otherwise noted, all chemicals and reagents were obtained from Fisher, Baxter Scientific, or Sigma.

Construction of Variant A. vinelandii Strains. Construction of *A. vinelandii nifB* and *nifH* deletion strains DJ1143 and DJ1165 (provided by Prof. Dennis Dean, Virginia Polytechnic Institute), which produce His-tagged Δ*nifB* and Δ*nifH* MoFe proteins, respectively, has been described earlier (*12*, *15*).

Cell Growth and Protein Sample Preparation. A. vinelandii mutant strains DJ1165 and DJ1143 were grown in 180 L batches in a 200 L New Brunswick fermentor on Burke's minimal medium supplemented with 2 mM ammonium acetate. The growth rate was measured by cell density at 436 nm. The His-tagged, FeMo cofactor-deficient MoFe proteins expressed by *A. vinelandii* DJ1165 (Δ*nifH* MoFe protein) and DJ1143 (Δ*nifB* MoFe protein) were purified as described earlier (*15*), except that the procedure was improved by (i) adding 10% glycerol to all buffers, (ii) limiting the purification process to less than 15 h, and (iii) performing cell rupture at less than 10000 psi. The complete occupancy of the P cluster or proposed P cluster precursor was confirmed by the presence of 17.0 ± 1.6 or 16.8 ± 1.3 mol of Fe/mol of Δ*nifB* or Δ*nifH* protein, respectively. All samples were prepared in a Ar-filled drybox (Vacuum Atmospheres, Hawthorne, CA) with an O_2 level of less than 3 ppm. Dithionite-reduced Δ*nifB* and Δ*nifH* MoFe proteins were in 25 mM Tris·HCl (pH 8.0), 10% glycerol, and 2 mM $Na_2S_2O_4$ (dithionite-reduced state). When prepared at University of California, Irvine, MoFe protein samples were oxidized by incubation with excess indigodisulfonate (IDS) for 30 min. IDS was subsequently removed by a single passage over an anion-exchange column (AG 1-X8; Bio-Rad, Hercules, CA), following a procedure described previously (*16*). IDS-oxidized and dithionite-reduced samples were concentrated in a Centricon-30 (Amicon) concentrator in anaerobic centrifuge tubes outside of the drybox. Some protein samples were frozen and shipped to Louisiana State University for spectral recording while others were placed into MCD cells and frozen prior to shipping. These latter MCD samples [up to 70 mg/mL protein in 150 μL of 25 mM Tris·HCl (pH 8.0) and 50% glycerol] were transferred into MCD sample cuvettes under anaerobic conditions and flash frozen in a pentane/liquid nitrogen slush. Oxidized Δ*nifB* MoFe protein samples prepared at Louisiana State University were made by slowly adding 1 mM thionine to

the sample in an anaerobic drybox (O_2 < 1.0 ppm) until the end point (i.e., faint blue color) was reached. Excess thionine was removed by passing the oxidized sample over a G-25 column containing anaerobic, but dithionite-free, buffer.

EPR Spectroscopy. All samples were prepared under anaerobic conditions using a Schlenck line. Protein samples were prepared under Ar in reducing Bis-Tris (pH 7.1) to a final volume of 350 μL and a final concentration of 10−30 mg/mL. EPR spectra were recorded on an X-band EPR spectrometer (Model EMX; Bruker, Billerica, MA) equipped with a liquid helium cryostat (Model ESR-900; Oxford, U.K.). Spectra were recorded at a temperature of 12 K, microwave frequency of 9.5 GHz, modulation amplitude of 12 G, time constant of 163 ms, and conversion time of 81.9 ms. Each spectrum represents the sum of three scans. Spin quantification of the $S = {}^1/_2$ EPR signal of the as-isolated Δ*nif*H MoFe protein was determined using the standard 0.1 mM CuEDTA. Double integration was performed on both $S = {}^1/_2$ EPR signals, and the percentage of unknown spins was calculated.

MCD Spectroscopy. MCD spectra were recorded with a CD spectropolarimeter (Model J-710; Jasco, MD) interfaced with a superconducting magnet (Model Spectromag 400-7T; Oxford, U.K.). Sample temperatures were monitored with a thin film resistance temperature sensor (Model CX1050-Cu-1-4L; Lakeshore, Westerville, OH) positioned directly (1 mm) above the sample cuvette. The linearity of the magnetic field was monitored with a calibrated Hall generator (Model HGCA-3020; Lakeshore, Westerville, OH) placed directly outside the superconducting magnet.

Sample cells were constructed of optical quality quartz (170−2200 nm, 1 mm path length, Model BS-1-Q-1; Buck Scientific, East Norwalk, CT; or Model SUV R-2001 or FUV; Spectrocell, Oreland, PA). Each cuvette was cut to the appropriate dimensions to fit the sample holder (1.8 cm × 0.45 cm), resulting in a sample volume of about 160 μL. All samples contained 50% glycerol to ensure the formation of an optical glass upon freezing.

All spectroscopic samples were prepared under anaerobic conditions. Previously frozen (as-isolated) samples were thawed in a 3.5 mL vial under anaerobic conditions on a Schlenck line. An MCD cuvette, positioned in the sample holder, was flushed for 30 s with He gas, filled with protein solution under a continuous flow of He gas, and rapidly frozen by lowering into the liquid He bath in the sample chamber of the Oxford magnet.

MCD spectra were recorded at a rate of 50 nm min^{-1} from 800 to 350 nm at a resolution of 2−10 nm. Since optical glasses formed at low temperature often generate a strain-induced background CD spectrum, the CD spectrum was recorded in zero magnetic field to determine whether the background signal was excessive. Those samples containing a significant CD spectrum were thawed and refrozen until the background signal reached an acceptable low level. To further eliminate interference by this signal, the corrected MCD spectrum was obtained for each sample by first recording the spectrum with the magnetic field in the normal direction and subtracting from it the spectrum with the field in the reversed direction. All spectral intensities were corrected for path length and sample concentration.

Analysis of Magnetization Data. Magnetization curves were recorded at a set wavelength and temperature while the magnetic field was linearly varied from 0 to 6 T at a rate of 0.1 A/s with a resolution of 2 s. MCD data were analyzed using a fit/simulation program created by Neese and Solomon (Stanford University) (*17*). The program allows the calculation of best-fit saturation magnetization curves using experimental data as a basis set and is valid for any spin state, half-integer or integer, at any specified temperature.

Experimental data were analyzed by fitting the spin Hamiltonian parameters and the effective transition moment products, M_{xy}^{eff}, M_{xz}^{eff} and M_{yz}^{eff}, with a scaling parameter $A_{satlim} = \gamma/4\pi S$, where γ is the magnetogyric ratio. The effective transition moment products represent the planes of polarization that reflect the anisotropy of the *g*-factors. Since the initial slope of the magnetization curve is dependent on the *g*-factors, the transition polarizations relate the transition dipole to the *g*-factor axes of a powder or randomly oriented sample. The spin parameters *g*-factor (*g*), axial zero-field splitting (*D*), and the rhombic distortion of the electronic environment (*E/D*) are based on the Hamiltonian

$$\hat{H} = \beta B g \hat{S} + D[\hat{S}_z^2 - (1/3)\hat{S}(\hat{S} + 1) + (E/D)(\hat{S}_x^2 - \hat{S}_y^2)] \quad (1)$$

which is the expression for energy of the Zeeman interaction and the correction to the energy of the individual spin states arising from spin−orbit coupling. At low temperatures (~1.6 K) the lowest energy state is predominantly populated and dictates the behavior of the magnetization curve. As the temperature is raised, the spectral parameters of excited states become increasingly important in the profile of the magnetization curve. Best-fit simulations of the experimental data were initially performed at the lowest temperature to aid the determination of the spectral parameters. Subsequent simulations of high-temperature data aided in the determination of the axial zero-field splitting, *D*.

MCD spectral intensities are the composite of three additive, contributing terms, called **A**, **B**, and **C**. The **A**-term arises from degenerate excited states, while the **C**-term arises from degenerate ground states. The **B**-term contribution does not require any degeneracy. Degeneracy of the ground or excited state will be removed in the presence of a magnetic field resulting in a derivative-shaped spectral inflection from the **A**- and **C**-terms. Furthermore, since the **C**-term is dependent on ground-state degeneracy, its intensity is regulated by the Boltzmann distribution of that state such that the intensity decreases with increasing temperature.

The **B**-term differs from the other two terms and is induced by ground- and excited-state mixing with the transition states. All molecules exhibit this effect. The **A**-term is temperature independent while the **B**-term is often temperature independent but can become temperature dependent when field-induced mixing occurs between low-lying states whose population is based on temperature.

RESULTS

EPR Spectroscopy. The hues of the two apo MoFe proteins differ (*15*), suggesting electronic differences between the metal clusters in the two proteins. To check this difference, the EPR spectra of the dithionite-reduced Δ*nifB* and Δ*nifH* MoFe proteins and oxidized Δ*nifB* and Δ*nifH* MoFe proteins were recorded. In agreement with previous measurements

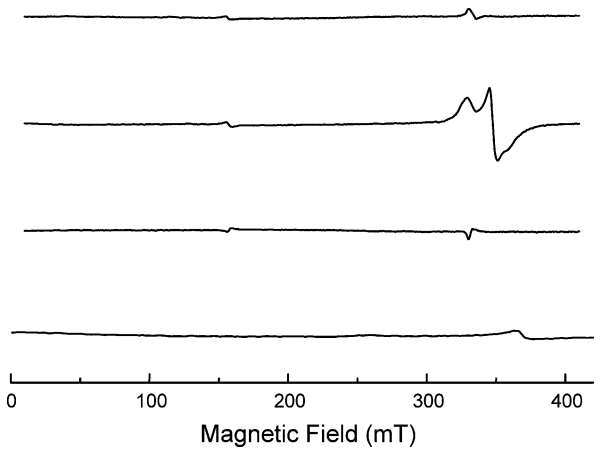

FIGURE 1: EPR spectra of (viewed top to bottom) oxidized Δ*nifH* MoFe protein (13 mg/mL), as-isolated Δ*nifH* MoFe protein (27 mg/mL), oxidized Δ*nifB* MoFe protein (13 mg/mL), and as-isolated Δ*nifB* MoFe protein (32 mg/mL). Samples were prepared and recorded as described in Materials and Methods.

(*12*, *15*) the dithionite-reduced Δ*nifB* MoFe protein is EPR silent while the as-isolated Δ*nifH* MoFe protein exhibits an axial $S = {}^1/_2$ EPR signal with $g_{\|} = 2.05$ and $g_{\perp} = 1.90$ (Figure 1). Spin integration of the $S = {}^1/_2$ EPR signal from the dithionite-reduced Δ*nifH* MoFe protein established it to represent about 0.7 spin/protein, in agreement with the previous work (*12*, *15*, *18*). Oxidation of the Δ*nifB* MoFe protein converts it into an EPR-active, absorption-shaped $g = 11.8$ signal best observed in a parallel mode cavity (*12*). On the other hand, oxidation of the Δ*nifH* MoFe protein converts it into an EPR-silent state in both parallel and perpendicular mode.

MCD Spectroscopy. (A) ΔnifB MoFe Protein. (1) Dithionite-Reduced ΔnifB MoFe Protein. The MCD spectrum of the dithionite-reduced Δ*nifB* MoFe protein (Figure 2A) is most noteworthy by its lack of features, decreasing gradually in intensity with increasing wavelength. The spectrum resembles more the absorption spectrum of this protein (*12*, *15*) than a typical MCD spectrum of a paramagnetic center. The spectrum also differs from typical MCD spectra in its constancy of intensity with temperature (1.63−9.30 K). In contrast, the holo MoFe protein, containing both the P cluster and FeMo cofactor, exhibits an MCD spectrum (Figure 2B) showing broad positive bands that decrease systematically in intensity with increasing temperature. This spectrum has been attributed to the paramagnetic ($S = {}^3/_2$) FeMo cofactor in the protein.

Magnetization curves were recorded at the maximum of a major positive band(s) in the MCD spectrum. Magnetization curves are plots of the MCD spectral intensity versus $\beta B/kT$, where β is the Bohr magneton, B is the magnetic flux density, k is the Boltzmann constant, and T is the absolute temperature. In paramagnetic systems, the shape of these curves is dominated by the temperature-dependent **C**-term of a paramagnetic transition. As a result of the Boltzmann distribution population of the Zeeman split ground state, the **C**-term is linearly dependent on magnetic flux/temperature at low magnetic flux and high temperature. This relationship is commonly referred to as the Curie law. As the magnetic flux increases and/or temperature decreases, the lowest state becomes the dominant populated level and, as such, the **C**-term becomes independent of the ratio B/T,

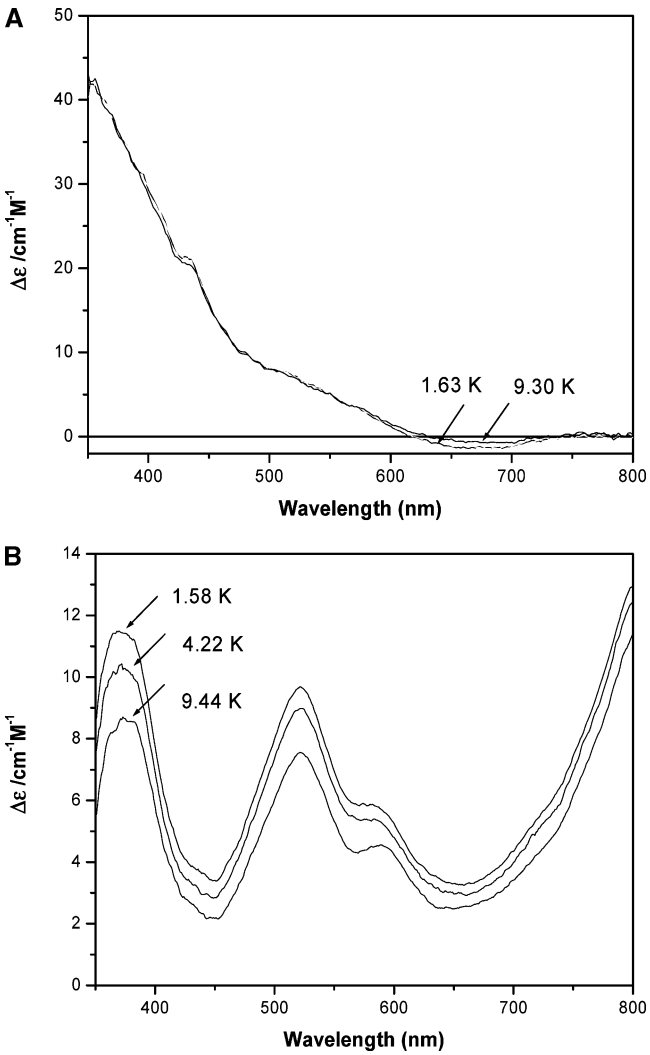

FIGURE 2: (A) MCD spectra of the as-isolated Δ*nifB* MoFe protein (32 mg/mL) at 6.0 T and temperatures of 1.63 and 9.30 K (spectrum at 4.22 K has been omitted for clarity). (B) MCD spectra of the as-isolated, wild-type MoFe protein at 6 T and temperatures of 1.58, 4.22, and 9.44 K. Samples were prepared and recorded as described in Materials and Methods.

asymptotically approaching a constant value called the saturation limit (A_{satlim}) (*19*−*21*).

Magnetization curves of the dithionite-reduced Δ*nifB* MoFe protein at temperatures of 1.63−9.30 K (Figure 3A) were recorded at 420 nm (this wavelength was arbitrarily chosen since the MCD spectrum shows no distinct maxima or minima). These curves are nearly linear and temperature dependent. When only plotted against the magnetic field (Figure 3B), the curves coalesce, reconfirming the temperature independence of the spectrum. This temperature independence is consistent with a diamagnetic ground state with a spectrum composed of only **A**- and/or **B**-terms. The absorption shape of the spectrum implies that it is dominated by a **B**-term contribution.

(2) Oxidized ΔnifB MoFe Protein. Upon oxidation, the Δ*nifB* MoFe protein exhibits an MCD spectrum (Figure 4) markedly different from that of the dithionite-reduced Δ*nifB* MoFe protein. The spectrum of the oxidized protein reveals dominant positive bands at 380 and 520 nm, a shoulder at 590 nm, and an intense broad band with maximum >800 nm. This spectrum is temperature dependent, decreasing in

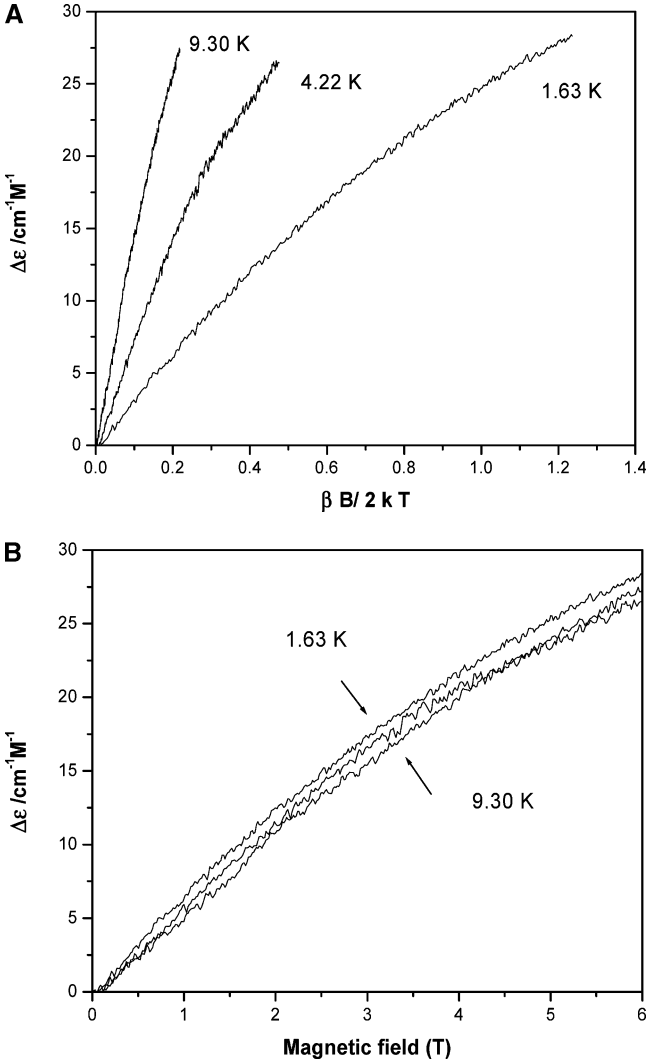

FIGURE 3: Magnetization curves of the as-isolated Δ*nifB* MoFe protein (32 mg/mL) recorded at 420 nm at temperatures of 1.63, 4.2, and 9.30 K. (A) Traditional magnetization curves showing the MCD intensity vs $\beta B/2kT$ at various temperatures. (B) MCD intensity curves plotted vs only the magnetic field intensity, illustrating the magnetic field dependency and temperature independency of the spectra.

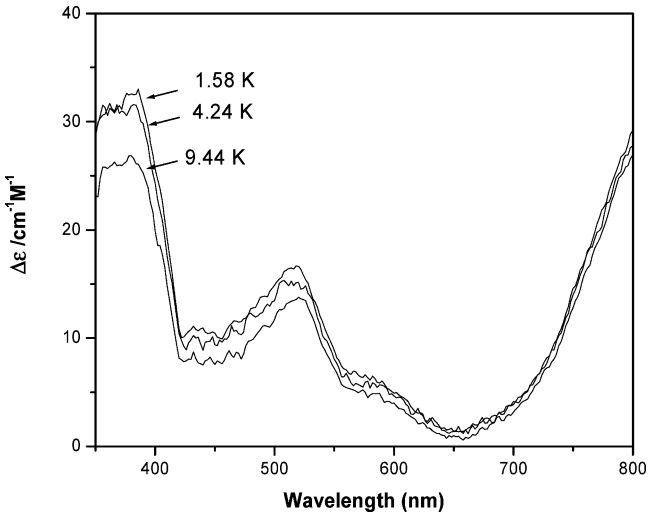

FIGURE 4: MCD spectra of the oxidized Δ*nifB* MoFe protein (13 mg/mL) recorded at 6.0 T and temperatures of 1.58, 4.22, and 9.44 K. Samples were prepared and recorded as described in Materials and Methods.

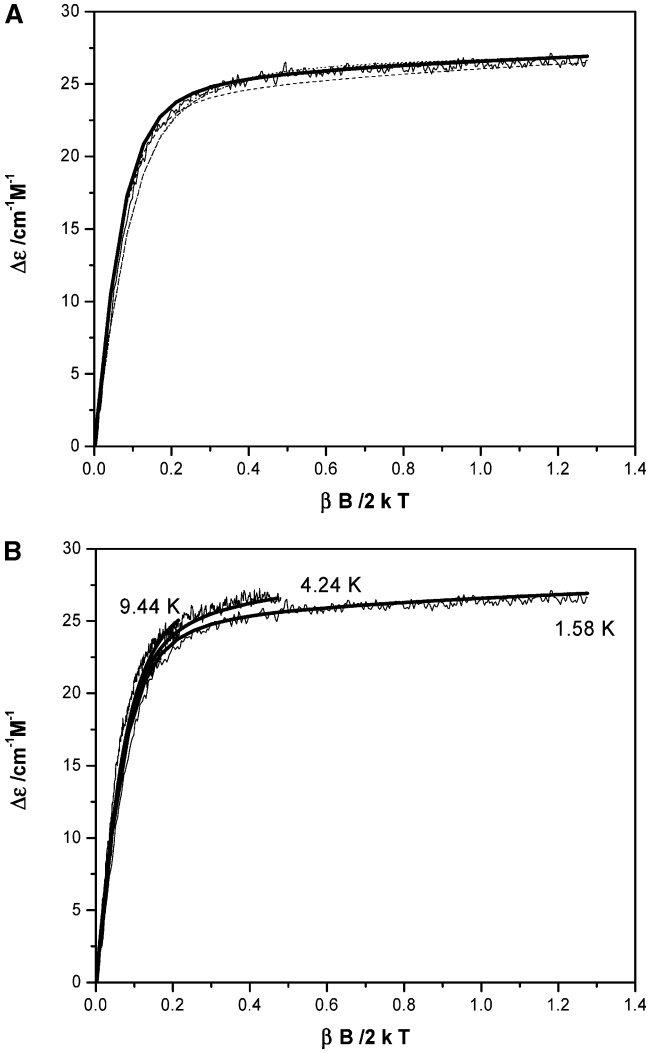

FIGURE 5: (A) Experimental and best-fit simulations of the magnetization curves performed at 790 nm for the oxidized Δ*nifB* MoFe protein (13 mg/mL) at 6.0 T and a temperature of 1.58 K. Simulation parameters are as follows: (•••) $S = 3$, $D = 4$ cm^{-1}, $E/D = 0.33$, $M_{xy}^{\text{eff}} = 0.35$, $M_{xz}^{\text{eff}} = 1.30$, and $M_{yz}^{\text{eff}} = 0.1$; (-•-) $S = 3$, $D = -3$ cm^{-1}, $E/D = 0.08$, $M_{xy}^{\text{eff}} = 1.25$, $M_{xz}^{\text{eff}} = 1.25$, and $M_{yz}^{\text{eff}} = -0.6$; (—) $S = 4$, $D = 4$ cm^{-1}, $E/D = 0.33$, $M_{xy}^{\text{eff}} = 0.75$, $M_{xz}^{\text{eff}} = 1.25$, and $M_{yz}^{\text{eff}} = 0.15$; (---) $S = 4$, $D = -3$ cm^{-1}, $E/D = 0.08$, $M_{xy}^{\text{eff}} = 1/19$, $M_{xz}^{\text{eff}} = 1.32$, and $M_{yz}^{\text{eff}} = -0.4$. (B) Experimental and simulated magnetization curves performed at 790 nm of the oxidized Δ*nifB* MoFe protein at 6.0 T and temperatures of 1.58, 4.22, and 9.44 K using the best-fit parameters for $S = 4$, $D = 4$ cm^{-1}, as listed above.

intensity with increasing temperature (1.58−9.44 K). The small rate of intensity decrease with increasing temperature suggests the presence of a high-spin, paramagnetic ground state while the presence of an EPR spectrum in parallel mode suggests an integer spin state.

A dramatic change is also observed from the nearly linear magnetization curves of the dithionite-reduced Δ*nifB* MoFe protein to the magnetization curves of the oxidized Δ*nifB* MoFe protein performed at 790 nm (Figure 5B). The magnetization curves of the oxidized Δ*nifB* MoFe protein exhibit a steep initial slope that rapidly approaches saturation. These curves are nested at different temperatures. Nesting refers to a change in the initial slope of the magnetization curve (increasing or decreasing) as the temperature increases. The source of nesting is usually the presence of low-lying

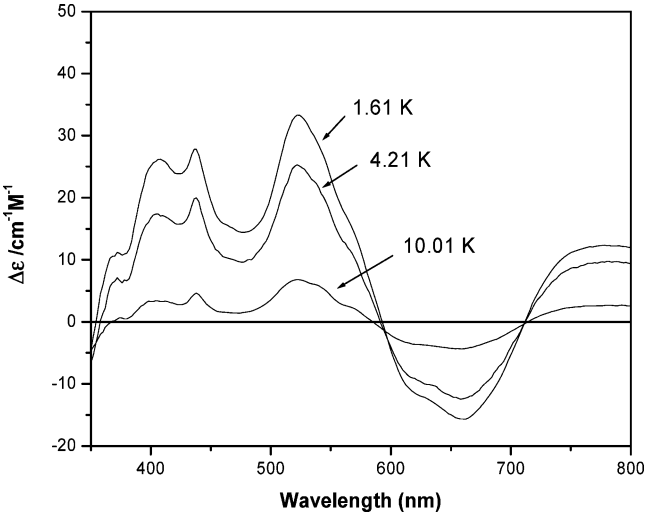

FIGURE 6: MCD spectra of the as-isolated Δ*nifH* MoFe protein (70 mg/mL) at 6 T and temperatures of 1.61, 4.21, and 10.01 K. Samples were prepared and recorded as described in Materials and Methods.

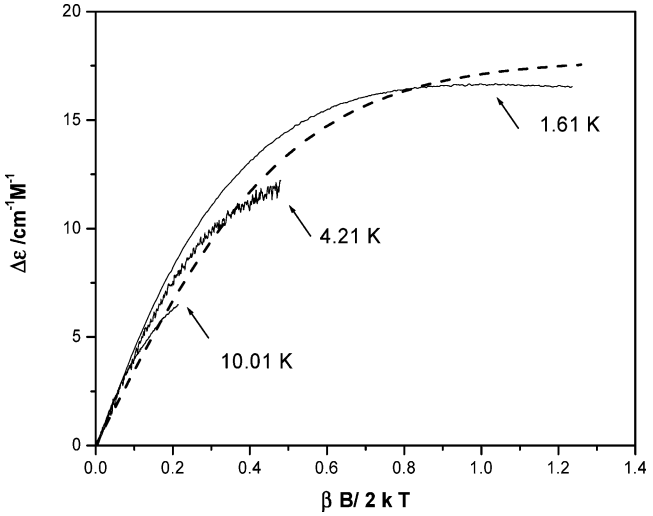

FIGURE 7: Best-fit simulation of the magnetization curve performed at 790 nm for the as-isolated Δ*nifH* MoFe protein (70 mg/mL) compared with the experimental data at temperatures of 1.61, 4.21, and 10.01 K. Simulation parameters are $S = {}^1/_2$, $M_{xy}^{\text{eff}} = 0.35$, $M_{xz}^{\text{eff}} = 1.30$, and $M_{yz}^{\text{eff}} = 0.1$.

paramagnetic excited states associated with different m_s energy levels of the spin system. The trend of the magnetization curves in Figure 5B shows positive nesting where the initial slope of each magnetization curve increases with increasing temperature (in negative nesting the slope decreases with increasing temperature). The extent of nesting reflects the magnitude of the zero-field splitting (zfs represented as D and E in eq 1) and is usually observed when the spin state $S > {}^1/_2$. The nesting observed in the MCD spectra of the Δ*nifB* MoFe protein along with the steep initial slope suggests a high-spin, paramagnetic ground state. This is consistent with the presence of a parallel mode EPR signal at g 11.8, implying an integer spin system, possibly $S = 3$ or 4.

(B) ΔnifH MoFe Protein. (1) Dithionite-Reduced ΔnifH MoFe Protein. The dithionite-reduced Δ*nifH* MoFe protein exhibits an MCD spectrum (Figure 6) with a wide range of positive bands at 404, 436, and 520 nm and a very broad maximum around 775 nm as well as positive shoulders around 537 and 567 nm. There is also a negative band centered at 660 nm and a negative shoulder at 615 nm. The intensities of all of these transitions are highly and uniformly temperature dependent, characteristic of a distinct paramagnetic ground state of low spin. This assignment is consistent with the EPR spectrum, which shows an axial $S = {}^1/_2$ signal.

The magnetization curves of the dithionite-reduced Δ*nifH* MoFe protein were recorded at 520 nm and temperatures of 1.61, 4.21, and 10.01 K (Figure 7). These curves exhibit classic magnetizations that are temperature dependent with a slow approach to saturation and negative nesting. Since $S = {}^1/_2$ states possess no low-lying excited states, nesting is not expected to be observed. The presence of nesting suggests an $S > {}^1/_2$ contribution to the spectrum, as discussed below.

(2) Oxidized ΔnifH MoFe Protein. The MCD spectrum of the oxidized Δ*nifH* MoFe protein (Figure 8), like that of the dithionite-reduced protein, exhibits a wide range of both positive and negative bands. Sharp positive bands are observed at 435, 467, 560, and 650 nm with a very broad band around 790 nm and a shoulder around 510 nm. Unlike the MCD spectrum of the oxidized Δ*nifB* MoFe protein,

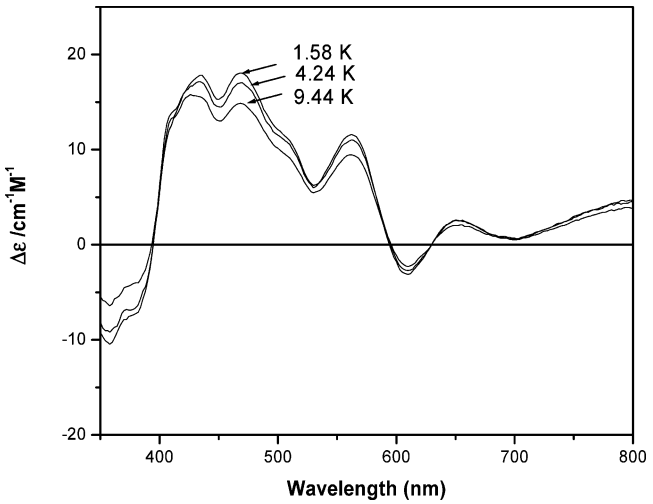

FIGURE 8: MCD spectra of the oxidized Δ*nifH* MoFe protein (34 mg/mL) at 6 T and temperatures of 1.58, 4.24, and 9.44 K. Samples were prepared and recorded as described in Materials and Methods.

which shows only broad positive bands (Figure 4), the spectrum of the Δ*nifH* MoFe protein also possesses a negative band at 610 nm. The intensities of all the bands in the oxidized Δ*nifH* MoFe protein uniformly decrease at a small rate as the temperature increases. Obviously, even though the oxidized Δ*nifH* MoFe protein is EPR silent, it possesses a paramagnetic ground state.

Magnetization curves at 790 nm (Figure 9) are distinctly different from those of the dithionite-reduced form. The curves of the oxidized Δ*nifH* MoFe protein possess a steep initial slope with a fast approach to saturation, analogous to the curves (Figure 5B) for the oxidized Δ*nifB* MoFe protein. However, these curves differ from those of the latter protein in having a downward slope after maximum magnetization is reached. The magnetization curves obtained at 560 nm (Figure 10) are similar in steepness to those at 790 nm but do not exhibit a downward slope. The initial steepness of both sets of magnetization curves of the oxidized Δ*nifH* MoFe protein suggests a high-spin state.

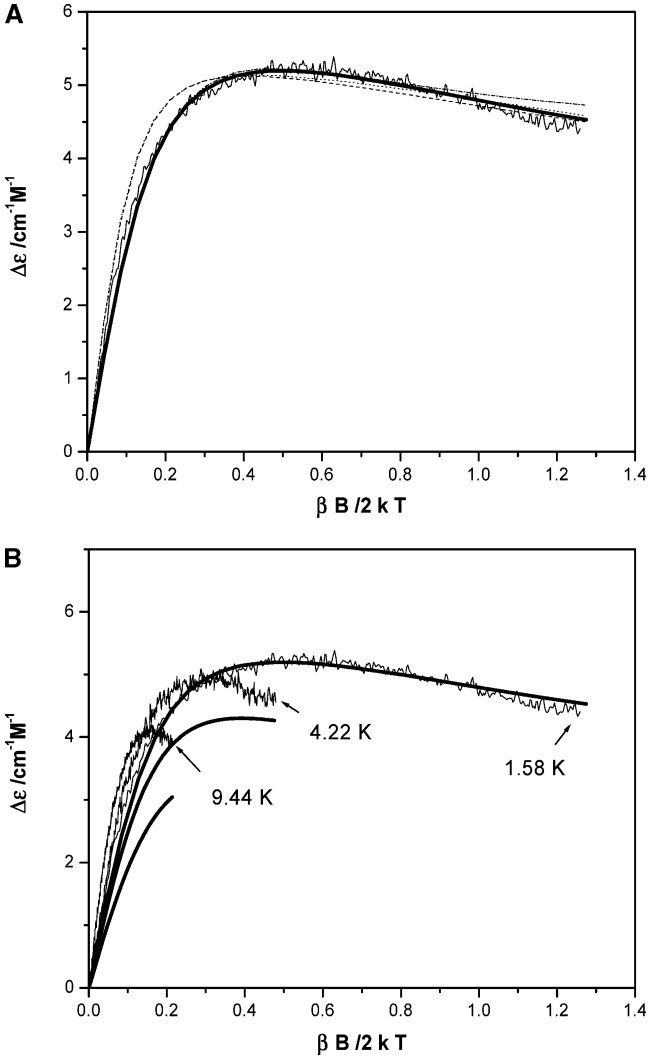

FIGURE 9: (A) Experimental and best-fit simulations of the magnetization curves performed at 790 nm for the oxidized Δ*nifH* MoFe protein (34 mg/mL) at 6.0 T and a temperature of 1.58 K. Simulation parameters are as follows: (•••) $S = 3$, $D = -3$ cm^{-1}, $E/D = 0.08$, $M_{xy}^{eff} = 0.24$, $M_{xz}^{eff} = 0.25$, and $M_{yz}^{eff} = -0.32$; (-•-) $S = 2$, $D = -3$ cm^{-1}, $E/D = 0.08$, $M_{xy}^{eff} = 0.28$, $M_{xz}^{eff} = 0.28$, and $M_{yz}^{eff} = -0.24$; (—) $S = 2$, $D = 2.82$ cm^{-1}, $E/D = 0.14$, $M_{xy}^{eff} = -0.33$, $M_{xz}^{eff} = 0.71$, and $M_{yz}^{eff} = 1.26$; (---) $S = 3$, $D = 3$ cm^{-1}, $E/D = 0.33$, $M_{xy}^{eff} = 0.24$, $M_{xz}^{eff} = 0.23$, and $M_{yz}^{eff} = -0.72$. (B) Experimental and simulated magnetization curves performed at 790 nm of the oxidized Δ*nifB* MoFe protein at 6.0 T and at temperatures of 1.58, 4.22, and 9.44 K.

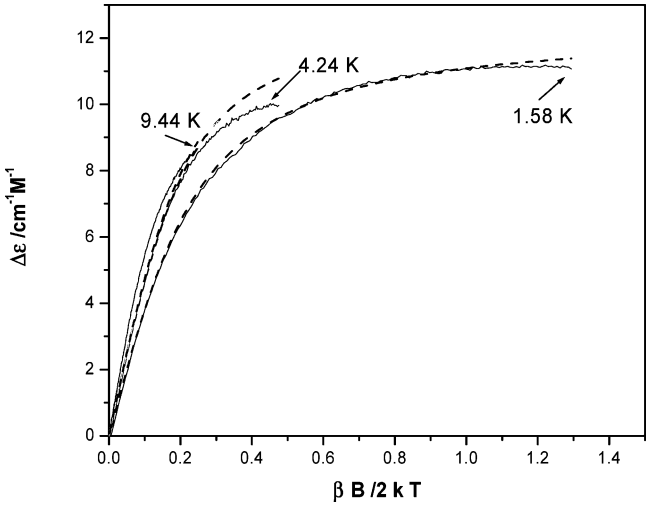

FIGURE 10: Experimental and simulated magnetization curves performed at 560 nm of oxidized Δ*nifH* MoFe protein at temperatures of 1.58, 4.24, and 9.44 K. Simulation parameters are $S = 2$, $D = 3.05$ cm^{-1}, $E/D = 0.17$, $M_{xy}^{eff} = 0.02$, $M_{xz}^{eff} = 0.89$, and $M_{yz}^{eff} = 0.94$.

DISCUSSION

This study reveals the MCD spectrum of the dithionite-reduced apo-MoFe protein, which arises from the P cluster without the interference of the FeMo cofactor. The spectrum confirms that the P cluster of the dithionite-reduced Δ*nifB* MoFe protein is diamagnetic. The $S = 0$ spin state is implied by the absence of temperature dependency of the spectral intensities and is consistent with the lack of EPR features. The MCD absorption at wavelengths below 450 nm is especially strong. This is important because it means that the spectrum that arises from the diamagnetic P cluster will have a significant contribution to the low-wavelength region to the MCD spectrum of the paramagnetic FeMo cofactor (Figure 2B) recorded in the dithionite-reduced MoFe protein, leading to a false representation of the cofactor's spectrum in the holo MoFe protein. The diamagnetic property of the P cluster in the Δ*nifB* MoFe protein is the same as that in the dithionite-reduced, holo MoFe protein (P^N state), as demonstrated in Mössbauer spectroscopic studies on the latter protein (*22*−*24*). The Mössbauer studies also show all eight Fe ions in the P cluster to be Fe^{2+} in the as-isolated protein. The study here, therefore, suggests the same valence characterization for the Fe ions in the P cluster in the dithionite-reduced Δ*nifB* MoFe protein from *A. vinelandii*. The MCD spectrum of the dithionite-reduced Δ*nifB* MoFe protein from *Klebsiella pneumoniae* has also been published (*25*). Unlike the sample used in this study, the protein from *K. pneumoniae* exhibited an $S = {}^1/_2$ EPR spectrum and a paramagnetic MCD spectrum. It has subsequently been shown (*26*) that the $S = {}^1/_2$ EPR signal observed with that protein originates from the paramagnetic P^+ state of the P cluster and not the diamagnetic reduced P^N state, as investigated here.

Following oxidation by either thionine or IDS, the Δ*nifB* MoFe protein exhibits an MCD spectrum with several broad temperature-dependent positive bands, indicative of a dominant **C**-term from a paramagnetic FeS center. This spectrum is essentially identical to that previously observed with the oxidized holo MoFe protein from *A. vinelandii* and *K. pneumoniae* as well as the oxidized Δ*nifB* MoFe protein from *K. pneumoniae* (*25*, *27*, *28*). Because the FeMo cofactor is diamagnetic in the oxidized holo MoFe protein, the MCD spectrum is dominated by the **C**-term of the paramagnetic P cluster in the P^{OX} state. The similarity of the MCD spectra that arises from the P clusters in all of these proteins suggests that oxidation of the Δ*nifB* MoFe protein converts its P clusters from the diamagnetic P^N state into a similar P^{OX} state.

The spin state of the P^{OX} has been the subject of much discussion. Mössbauer and parallel-mode EPR studies on the holo MoFe protein (*24*) suggest a spin state of $S = 3.0$ or 4.0. However, both spectroscopic techniques have difficulty determining spectral and spin-state parameters (e.g., *D*, *E*/*D*, and *S*) of integer states. The Mössbauer studies suggest the electronic ground state of P^{OX} is a nearly degenerate doublet of an integer spin system while the EPR spectrum (inflection

Table 1: Parameters of the Best-Fit Simulations

MoFe protein	S	D[a] (cm^{-1})	E/D[b]	g-factors	polarization[c] M_{xy}^{eff}	M_{xz}^{eff}	M_{yz}^{eff}
as-isolated Δ*nifH*	$^1/_2$	NA	NA	2.05, 1.98, 1.90	0.35	1.30	0.10
oxidized Δ*nifH*, $\lambda = 790$ nm	2	2.82	0.14	2.0023	−0.33	0.71	1.26
oxidized Δ*nifH*, $\lambda = 560$ nm	2	3.05	0.17	2.0023	−0.02	0.89	0.94
as-isolated Δ*nifB*	0	NA	NA	NA		NA	
oxidized Δ*nifB*, $\lambda = 790$ nm	4	4.00	0.33	2.0023	0.75	1.32	−0.40

[a] Uncertainty ±0.05. [b] Uncertainty ±0.02. [c] Uncertainty ±0.08.

at g 11.8 in parallel mode) possibly arises from an excited-state $m_s = \pm 3.0$ transition. The dominant **C**-term of the MCD spectrum (Figure 4) at very low temperatures is often taken to mean $D < 0$. These interpretations are less valid for a system of high rhombicity.

To help to clarify these interpretations, we undertook a simulation study of the magnetization curves of the oxidized Δ*nifB* MoFe protein for different integer spin states. Best-fit simulations (Figure 5A) of the 1.58 K magnetization curve were determined for $S = 2.0$, 3.0, and 4.0 using both positive and negative D while varying both E/D (0 to $^1/_3$) and the effective transition moment products, M_{xy}^{eff}, M_{xz}^{eff}, and M_{yz}^{eff}. As an initial approximation, we assumed that the **B**-terms of the ground and excited states were small compared to the ground-state **C**-term. This assumption tends to be valid for high-spin states but can break down for lower spin states ($S \leq 2$). Of the three spin states, $S = 2$ was the only one that could not simulate the data using $D > 0$. Even with $D < 0$, the simulation using $S = 2$ is very poor. Both $S = 3$ and $S = 4$, with either positive or negative D, provide adequate simulations of the data, with $S = 4$, $D > 0$ providing the best least fair fit (Table 1). The close fit is true for the lowest temperature data as well as the data at elevated temperatures (Figure 5B). While the values of D and E/D for each spin state are only approximations for the oxidized Δ*nifB* MoFe protein, our simulations define the range of acceptable values and show the possibility of $D > 0$.

The dithionite-reduced Δ*nifH* MoFe protein is clearly paramagnetic, exhibiting the EPR spectrum of an axial $S = ^1/_2$ spin state. The MCD spectrum of this protein (Figure 6) has the classic profile of a $[4Fe\text{-}4S]^+$ cluster and is similar to the spectrum of the $[4Fe\text{-}4S]^+$ cluster in the NifEN protein (*29*). This characterization is consistent with a recent K-edge Fe-EXAFS study on the Δ*nifH* MoFe protein, which found Fe−S and Fe−Fe distances similar to conventional $[4Fe\text{-}4S]^+$ clusters (*14*). The magnitude of the molar MCD intensity of approximately 35 $\Delta\epsilon$ M^{-1} cm^{-1} at 520 nm implies the presence of less than 1.0 $[4Fe\text{-}4S]^+$ cluster per Δ*nifH* MoFe protein (*30*, *31*) and is consistent with the EPR spin quantification of 0.7 spin per protein. The low-spin concentration suggests that the P cluster precursors in the dithionite-reduced state of the Δ*nifH* MoFe protein are not fully poised in the $[4Fe\text{-}4S]^+$ state.

The spectral parameters of an $S = ^1/_2$ state ($g = [2.05, 1.90, 1.90]$ and, by definition, $D = 0$, $E/D = 0$) greatly simplify the simulation of its magnetization curves. Furthermore, because the g anisotropy is small, variations in the effective transition moment products have only minor effect on the shape of the magnetization curve. In spite of this, Figure 7 shows that the simulation of an $S = ^1/_2$ system does not provide a good fit of the data, implying the presence of another spectral component, possibly associated with a higher spin paramagnetic state or maybe a dominant **B**-term contribution. The presence of mixed spin states is not unusual in $[4Fe\text{-}4S]^+$ clusters and may explain the EPR spectral data, which show the $S = ^1/_2$ signal representing only about 70% of the dithionite-reduced Δ*nifH* MoFe protein. The EPR spectrum of a second spin state has not been observed.

The MCD and EXAFS studies are consistent with the presence of paramagnetic $[4Fe\text{-}4S]^+$ clusters in the dithionite-reduced Δ*nifH* MoFe protein, presumably equally distributed between the two equivalent P cluster sites. The EXAFS study further suggests that all of the Fe atoms are in [4Fe-4S]-like clusters. The Fe quantification of about 16 per protein implies two [4Fe-4S]-like clusters per P cluster site where one of the two is in the $[4Fe\text{-}4S]^+$ state in the dithionite-reduced state of the Δ*nifH* MoFe protein. Assuming that this representation is correct, we can predict the structural arrangement of the other cluster in each half.

In the dithionite-reduced protein, only the $S = ^1/_2$ signal of the $[4Fe\text{-}4S]^+$ cluster is observed and is unperturbed by neighboring spin interactions. Therefore, either the second [4Fe-4S]-like cluster is diamagnetic or paramagnetic in an EPR-silent state. If paramagnetic, the second cluster must be distant (>12 Å) from the $[4Fe\text{-}4S]^+$ cluster, since no spin perturbations are observed in the EPR spectrum. Because it is unlikely that the second cluster is this far from the $[4Fe\text{-}4S]^+$ cluster, we favor the first description.

Upon oxidation, the Δ*nifH* MoFe protein becomes EPR silent in both perpendicular and parallel modes. Most surprisingly, the MCD spectrum (Figure 8) clearly shows a paramagnetic ground state. This spectrum is more similar to that of the dithionite-reduced protein (Figure 6), possessing both positive and negative inflections, than it is to the broad, all positive spectrum of the oxidized Δ*nifB* MoFe protein (Figure 4). Obviously the oxidized Δ*nifB* and Δ*nifH* MoFe proteins have different cluster and electronic structures.

The fact that the oxidized Δ*nifH* MoFe protein is EPR silent, yet paramagnetic, suggests a low-value, integer spin state of the present clusters. This statement is based on the general observation that the separation between the energy levels of $S = 1$ or 2 states tends to be large such that transitions between these levels are usually unobservable at X-band frequencies. Energy level separations dramatically decrease in higher spin states, often making transitions observable. In agreement with this, simulations of magnetization curves at both 520 and 790 nm are best fit with $S = 2$ and $D \approx 3$ cm^{-1} (Figure 10) with moderate rhombicity ($E/D = 0.17$ and 0.15, respectively).

The presence of paramagnetism in the oxidized Δ*nifH* MoFe protein definitely rules out the possibility that each half of the oxidized protein contains a pair of $[4Fe\text{-}4S]^{2+}$

clusters, since such clusters are always diamagnetic. This means that the clusters are unique and do not behave like conventional ferredoxin-like clusters, which would be in the diamagnetic $[4Fe\text{-}4S]^{2+}$ state under these oxidizing conditions. A consequence of this is that the dithionite-reduced protein does not contain the cluster pair $[4Fe\text{-}4S]^{+}$ and $[4Fe\text{-}4S]^{2+}$ in each protein half, since oxidation of this cluster pair would generate a pair of $[4Fe\text{-}4S]^{2+}$ clusters, contrary to our MCD data. One possibility is that both clusters in the oxidized protein are neighboring half-integer spin clusters (possibly two $[4Fe\text{-}4S]^{+}$ clusters) and, due to spin−spin interaction, couple to produce an integer spin system. Another possibility is that both clusters have integer spin yet are well separated. Our data cannot distinguish between these two possibilities but again favor the first interpretation. It is important to note that our data also rule out the possibility of the two clusters in the oxidized protein be well-separated (>12 Å), half-integer clusters (such as two $[4Fe\text{-}4S]^{+}$). Such an arrangement would exhibit an EPR spectrum resulting from the overlap of the spectra of the two separate clusters. The clusters in the Δ*nifH* MoFe protein, therefore, are paramagnetic when oxidized and have redox and/or electronic properties significantly different from normal ferredoxins. This is consistent with the properties of the P clusters, which exist in the all ferrous state in the as-isolated protein.

Purified Δ*nifH* MoFe protein can only be activated up to 9−13% of the wild-type activity upon addition of isolated FeMo cofactor, Fe protein, and MgATP (*32*). This could be explained by the presence of 87−91% damaged P cluster species in the Δ*nifH* MoFe protein. However, this is a highly unlikely scenario because (i) Δ*nifH* MoFe protein prepared from different batches of purifications showed reproducible iron content as well as XAS/EXAFS and EPR spectroscopic properties (this cannot be the case if the P cluster species in the Δ*nifH* MoFe protein represents a form of P cluster that is randomly damaged during preparation) and (ii) Δ*nifH* MoFe protein can be fully activated, in crude extracts of *A. vinelandii nifH* deletion strains DJ1165 (data not shown) or DJ54 (*18*, *33*, *34*), upon addition of isolated FeMo cofactor, Fe protein, and MgATP. This observation indicates that additional factors and/or components are required for the complete reconstitution of Δ*nifH* MoFe protein (*18*) and explains the relatively low level of reconstitution of purified Δ*nifH* MoFe protein when only purified Fe protein is added (*32*). Nevertheless, the fact that the Δ*nifH* MoFe protein can be fully activated strongly points to the possibility that the P cluster species in the Δ*nifH* MoFe protein represents a physiologically relevant snapshot during P cluster assembly (i.e., precursor) rather than an irreversibly damaged form of the P cluster.

CONCLUSION

The MCD spectrum of the P cluster in the Δ*nifB* MoFe protein is consistent with past X-ray diffraction and spectroscopic studies on this protein, showing it to be diamagnetic in the dithionite-reduced state and possessing an spectrum identical to that of the P cluster in the holo MoFe protein in the oxidized state. The MCD spectrum of the dithionite-reduced Δ*nifH* MoFe protein clearly shows the presence of $[4Fe\text{-}4S]^{+}$ clusters, consistent with the $S = {}^{1}/_{2}$ EPR spectrum. Oxidation of this latter protein generates an EPR-silent species while the MCD spectrum reveals a paramagnetic ground state, presumably of integer spin. The paramagnetism of the oxidized protein rules out the existence of neighboring $[4Fe\text{-}4S]^{2+}$ clusters, which are always diamagnetic. By inference, the dithionite-reduced protein does not contain the $[4Fe\text{-}4S]^{+}/[4Fe\text{-}4S]^{2+}$ pair in each half. Therefore, the Δ*nifH* MoFe protein contains an unusual pair of [4Fe-4S]-like clusters with unusual redox properties.

ACKNOWLEDGMENT

We acknowledge Professor Dennis Dean of Virginia Polytechnic Institute and State University for kindly providing us *A. vinelandii* strains DJ1143 and DJ1165.

REFERENCES

1. Burgess, B. K., and Lowe, D. J. (1996) Mechanism of Molybdenum Nitrogenase, *Chem. Rev. 96*, 2983−3011.
2. Howard, J. B., and Rees, D. C. (1996) Structural Basis of Biological Nitrogen Fixation, *Chem. Rev. 96*, 2965−2982.
3. Smith, B. E. (1999) Structure, Function and Biosynthesis of the Metallosulfur Clusters in Nitrogenase, *Adv. Inorg. Chem. 47*, 159−218.
4. Rees, D. C., and Howard, J. B. (2000) Nitrogenase: Standing at the Crossroads, *Curr. Opin. Chem. Biol. 4*, 559−566.
5. Christiansen, J., Dean, D. R., and Seefeldt, L. C. (2001) Mechanistic Features of the Mo-Containing Nitrogenase, *Annu. Rev. Physiol. Plant Mol. Biol. 52*, 269−295.
6. Igarashi, R. Y., and Seefeldt, L. C. (2003) Nitrogen Fixation: The Mechanism of the Mo-dependent Nitrogenase, *Crit. Rev. Biochem. Mol. Biol. 38*, 351−384.
7. Seefeldt, L. C., Dance, I. G., and Dean, D. R. (2004) Substrate Interactions with Nitrogenase: Fe versus Mo, *Biochemistry 43*, 1401−1409.
8. Peters, J. W., Stowell, M. H. B., Soltis, S. M., Finnegan, M. G., Johnson, M. K., and Rees, D. C. (1997) Redox-Dependent Structural Changes in the Nitrogenase P-Cluster, *Biochemistry 36*, 1181−1187.
9. Einsle, O., Tezca, F. A., Andrade, S. L. A., Schmid, B., Yoshida, M., Howard, J. B., and Rees, D. C. (2002) Nitrogenase MoFe-Protein at 1.16 Å Resolution: A Central Ligand in the FeMo-Cofactor, *Science 297*, 1696−1700.
10. Mayer, S. M., Lawson, D. M., Gormal, C. A., Roe, S. M., and Smith, B. E. (1999) New Insights into Structure-Function Relationships in Nitrogenase: A 1.6 Å Resolution X-Ray Crystallographic Study of *Klebsiella pneumoniae* MoFe-protein, *J. Mol. Biol. 292*, 871−891.
11. Dos Santos, P. C., Dean, D. R., Hu, Y., and Ribbe, M. W. (2004) Formation and Insertion of the Nitrogenase Iron-Molybdenum Cofactor, *Chem. Rev. 104*, 1159−1173.
12. Christiansen, J., Goodwin, P. J., Lanzilotta, W. N., Seefeldt, L. C., and Dean, D. R. (1998) Catalytic and Biophysical Properties of a Nitrogenase Apo-MoFe Protein Produced by a *nifB*-Deletion Mutant of *Azotobacter vinelandii*, *Biochemistry 37*, 12611−12623.
13. Schmid, B., Ribbe, M., Einsle, O., Yoshida, M., Thomas, L. M., Dean, D. R., Rees, D. C., and Burgess, B. K. (2002) Structure of a Cofactor-Deficient Nitrogenase MoFe Protein, *Science 296*, 352−356.
14. Campbell, M., Hu, Y., Naderi, F., Ribbe, M. W., Hedman, B., and Hodgson, K. O. (2004) Comparison of Iron-Molybdenum Cofactor-deficient Nitrogenase MoFe Proteins by X-ray Absorption Spectroscopy—Implication for P-cluster Biosynthesis, *J. Biol. Chem. 279*, 28276−28282.
15. Ribbe, M., Hu, Y., Guo, M., Schmid, B., and Burgess, B. K. (2002) The FeMoco-Deficient MoFe Protein Produced by the *nifH* Deletion Strain of *Azotobacter vinelandii* Shows Unusual P-Cluster Features, *J. Biol. Chem. 277*, 23469−23476.
16. Bursey, E. H., and Burgess, B. K. (1998) The Role of Methionine 156 in Cross-Subunit Nucleotide Interactions in the Iron Protein of Nitrogenase, *J. Biol. Chem. 273*, 29678−29685.
17. Neese, F., and Solomon, E. I. (1999) MCD C-Term Signs, Saturation Behavior, and Determinationof Band Polarizations in Ramdomly Oriented Systems with $S \geq {}^{1}/_{2}$. Applicaitons to $S = {}^{1}/_{2}$ and $S = {}^{5}/_{2}$, *Inorg. Chem. 38*.

18. Gavini, N., Ma, L., Watt, G., and Burgess, B. K. (1994) Purification and Characterization of a FeMo Cofactor-Deficient MoFe Protein, *Biochemistry 33*, 11842−11849.
19. Stephens, P. J. (1976) Magnetic Circular Dichroism, *Adv. Chem. Phys. 35*, 197−264.
20. Phiepho, S. B., and Schatz, P. N. (1983) *Group Theory in Spectroscopy with Applications to Magnetic Circular Dichroism*, Wiley, New York.
21. Schatz, P. N., and McCaffrey, A. J. (1969) The Faraday Effect, *Q. Rev. Chem. Soc. 23*, 552−584.
22. Zimmermann, R., Münck, E., Brill, W. J., Shah, V. K., Henzl, M. T., Rawlings, J., and Orme-Johnson, W. H. (1978) Nitrogenase X: Mössbauer and EPR Studies on Reversibly Oxidized MoFe Protein from *Azotobacter vinelandii* OP, *Biochim. Biophys. Acta 536*, 185−207.
23. Huynh, B. H., Emptage, M. H., and Münck, E. (1978) Mössbauer Study of Cytochrome c_2 from *Rhodospirillum rubrum*, *Biochim. Biophys. Acta 534*, 295−306.
24. Surerus, K. K., Hendrich, M. P., Christie, P. D., Rottgardt, D., Orme-Johnson, W. H., and Münck, E. (1992) Mössbauer and Integer-Spin EPR of the Oxidized P-Clusters of Nitrogenase: P^{ox} is a Non-Kramers System with a Nearly Degenerate Ground Doublet, *J. Am. Chem. Soc. 114*, 8579−8590.
25. Robinson, E., A., Richards, A. J. M., Thomson, A. J., Hawkes, T. R., and Smith, B. E. (1984) Low-Temperature Magnetic-Circular-Dichroism Spectroscopy of the Iron-Molybdenum Cofactor and the Complementary Cofacter-Less MoFe protein of *Klebsiella pneumoniae* nitrogenase, *Biochem. J. 219*, 495−503.
26. Tittsworth, R. C., and Hales, B. J. (1993) Detection of EPR Signals Assigned to the 1-equiv-Oxidized P-Clusters of the Nitrogenase MoFe-Protein from *Azotobacter vinelandii*, *J. Am. Chem. Soc. 115*, 9763−9767.
27. Johnson, M. K., Thomson, A. J., Robinson, A. E., and Smith, B. E. (1981) Characterization of the Paramagnetic Centres of the Molybdenum-Iron Protein of Nitrogenase from *Klebsiella pneumoniae* Using Low-Temperature Magnetic Circular Dichroism Spectroscopy, *Biochim. Biophys. Acta 671*, 61−70.
28. Morningstar, J. E., Johnson, M. K., Case, E. E., and Hales, B. J. (1987) Characterization of the Metal Clusters in the Nitrogenase Molybdenum-Iron and Vanadium-Iron Proteins of *Azotobacter vinelandii* Using Magnetic Circular Dichroism Spectroscopy, *Biochemistry 26*, 1795−1800.
29. Goodwin, P. J., Agar, J. N., Roll, J. T., Roberts, G. P., Johnson, M. K., and Dean, D. R. (1998) The *Azotobacter vinelandiii* NifNE Complex Contains Two Identical [4Fe-4S] Clusters, *Biochemistry 37*, 10420−10428.
30. Conover, R. C., Kowal, A. T., Fu, W., Park, J.-B., Aono, S., Adams, M. W. W., and Johnson, M. K. (1990) Spectroscopic Characterization of the Novel Iron-Sulfur Cluster in *Pyrococcus furiosus* Ferredoxin, *J. Biol. Chem. 265*, 8533−8541.
31. Onate, Y. A., Finnegan, M. G., Hales, B. J., and Johnson, M. K. (1993) Variable Temperature Magnetic Circular Dichroism Studies of Reduced Nitrogenase Iron Proteins and $[4Fe\text{-}4S]^+$ Synthetic Analog Clusters, *Biochim. Biophys. Acta 1164*, 113−123.
32. Hu, Y., Corbett, M. C., Fay, A. W., Webber, J. A., Hedman, B., Hodgson, K. O., and Ribbe, M. W. (2005) Nitrogenase Reactivity with P-cluster Variants, *Proc. Natl. Acad. Sci. U.S.A. 102*, 13825−13830.
33. Tal, S., Chun, T. W., Gavini, N., and Burgess, B. K. (1991) The delta nifB (or delta nifE) FeMo cofactor-deficient MoFe protein is different from the delta nifH protein, *J. Biol. Chem. 266*, 10654−10657.
34. Robinson, A. C., Chun, T. W., Li, J. G., and Burgess, B. K. (1989) Iron-molybdenum cofactor insertion into the Apo-MoFe protein of nitrogenase involves the iron protein-MgATP complex, *J. Biol. Chem. 264*, 10088−10095.
35. Ribbe, M., Gadkari, D., and Meyer, O. (1997) N_2 Fixation by *Streptomyces thermoautotrophicus* Involves a Molybdenum-Dinitrogenase and a Manganese-Superoxide Oxidoreductase That Couple N_2 Reduction to the Oxidation of Superoxide Produced from O_2 by a Molybdenum-CO Dehydrogenase, *J. Biol. Chem. 272*, 26627−26633.
36. Rubio, L. M., and Ludden, P. W. (2005) Maturation of Nitrogenase: A Biochemical Puzzle, *J. Bacteriol. 187*, 405−414.

BI061697P